The Measurement of Geopotential Heights by GPS Radio Occultation†

Stephen S. Leroy‡
NASA/Jet Propulsion Laboratory

Submitted to: *J. Geophys. Res.*, April ?, 1996

Abstract

Geopotential heights of constant pressure surfaces are retrieved from GPS radio occultation data. In order to assess accuracy, a subset of data obtained by GPS/MET during spring 1995 and summer 1995 are compared to the output of the ECMWF global model. The root-mean-square measurement error is 20 meters till'oll@loul the upper troposphere and lower stratosphere. Furthermore, the ECMWF global model contains enhanced errors in the Southeast Pacific. In probing the data for potential utility in climate studies, a Bayesian interpolation technique is used to map the geopotential height fields in the upper troposphere during the summer. Despite limitations of the GPS/MET data set, the global average 300 mbar geopotential height over a two week period in summer 1995 is determined with an accuracy of 7 meters. By obtaining greater coverage and partially resolving synoptic variability, a future constellation of 16 orbiting receivers could obtain global average geopotential height estimates in the upper troposphere with an accuracy of 1 meter each day. Accuracy would be somewhat worse for regional studies, except in the tropics where synoptic variability is depressed.

1. Introduction

Measuring geopotential heights of constant pressure surfaces has become a common approach to detecting global warming (Wallace and Zhang 1993 and references therein). This technique is attractive because, in a global warming scenario, thermal expansion raises the height of constant pressure surfaces, thus affording a means to measure bulk temperature of the troposphere. The measurements commonly cited are generated by assimilation models whose primary source of geopotential information is radiosondes. Because there are so few radiosonde sites in the Southern Hemisphere, climate analyses of geopotential heights are mostly restricted to the Northern Hemisphere. Moreover, the climate as recorded by radiosondes and derivative products is difficult to interpret because of changes in radiosonde instrumentation (Gaffen 1994) and analysis technique over time (Lambert 1990).

Whether a bulk measurement of atmospheric temperature is the best method to detect global warming has been questioned by Barnett and Schlesinger (1987) because the model-predicted "fingerprint" of warming in the mid-troposphere is similar to the naturally occuring interannual variability. They nonetheless state that a space-based measurement of mid-troposphere temperature is desireable in a suite of measurements necessary to positively detect CO_2-induced warming.

† Contribution ? of the Jet Propulsion Laboratory of the California Institute of Technology

‡ *Address:* Earth and Space Sciences Division, mail stop 183-335, Jet Propulsion Laboratory, California Institute of Technology, Pasadena, California 91109

Spencer and Christy (1990, 1992a,b) have used the microwave sounding units (MSU) aboard a series of NOAA satellites to measure tropospheric-generated radiances. The second channel of the MSU samples the 53.74-GHz oxygen line. The weighting function for this channel spans much of the troposphere, and the brightness temperature in this channel is only negligibly impacted by water and clouds (Spencer et al. 1990). Even though an intercomparison of monthly-integrated brightness temperatures between two NOAA satellites during a two year overlap showed no instrument drift and that calibration errors are less than 0.01°C, nevertheless, MSU-measured brightness temperatures and surface air temperatures showed trends different by 0.1°/decade over the period of 1979 through 1990, which provoked a lively exchange between the authors of the respective analyses (Christy and Spencer 1995, Hansen et al. 1995). It became clear in this exchange that the MSU channel 2 brightness temperature is probably a more complicated quantity than an average tropospheric temperature.

In this paper a new approach to measuring bulk tropospheric temperatures from space is presented. It is done by measuring geopotential heights of constant pressure surfaces by radio occultation using the global positioning system (GPS). Because the fundamental quantity in the measurement is light travel time, it is insensitive to calibration difficulties and instrument drift common to radiometric measurements. This quality also makes the measurement insensitive to instrument generation. Secondly, because the physical bases of the measurements are fundamentally different, occultations are characterized by significantly finer vertical resolution than nadir sounding instruments are: occultations have less than 1-km vertical resolution whereas nadir sounders yield 3-7-km vertical resolution (Chahine et al. 1984). Finally, the potential of this technique is enhanced because the experimental cost is that of a GPS receiver, which is light enough to be carried as a secondary payload on many launches of opportunity.

Radio occultation has been previously used to retrieve some of the most accurate temperature profiles available for the atmospheres of the outer planets (Lindal 1981, Tyler et al. 1982, Lindal et al. 1987, 1992). For the terrestrial atmosphere, obtaining temperature profiles using radio occultation can be done on a large scale using the GPS satellites as the active radio source (Melbourne et al. 1988, 1994). Whereas just a few such profiles exist for the extraterrestrial atmospheres, with the GPS system and a GPS receiver in a low Earth orbit (LEO) one should be able to collect several hundred profiles of the Earth's atmosphere every day.

The methodology of GPS occultation has been amply and ably discussed elsewhere (e.g. Hardy et al. 1994, Hajj et al. 1995, Kursinski et al. 1996b), but a brief description is warranted here. In a GPS occultation, the orbiting GPS receiver measures the Doppler shift of a GPS transmission as a function of time. With highly accurate knowledge of the positions and velocities of the transmitting GPS satellite and the flight receiver and an assumption of spherical symmetry of the atmosphere, one can retrieve the bending angle and the impact parameter of the radio beam as a function of time. A continuous measurement of this bending angle and impact parameter can be inverted for the refractive index of the refracting medium as a function of altitude. In turn, the refractive index is determined by a combination of density and water vapor within the neutral atmosphere. There is little enough water vapor in the upper troposphere that there is a direct relationship between the refractive index and the atmospheric density. In this region the pressure can be estimated by integrating the atmospheric density above the level of interest via the hydrostatic equation. Subsequently, the equation of state is used to determine temperature as a function of pressure.

GPS occultation measures refractivity as a function of absolute position, a characteristic which can be used to calculate geopotential heights. A vertical integration of density gives pressure also as a function of absolute position. In the retrieval process, the determination of absolute position is dependent only on knowledge of transmitter and receiver positions and an assumption of spherical symmetry not on any spacecraft pointing measurements. This capability is not shared with other nadir sounding instruments, for which pressure is the only available vertical coordinate.

Before measurements of geopotential heights can be used in assimilation models or global change analysis, it is necessary to understand the errors associated with such measurements. Kursinski et al. (1996b) have shown that the geopotential height can be retrieved with a theoretical accuracy of 7 meters, the primary error sources being an ionospheric correction to measured bending angles and density inhomogeneities along the beam's path. With occultation data from GPS/MET, a proof-of-concept experiment for GPS occultation (Ware et al. 1996, Kursinski et al. 1996a), it is possible to perform an experimental study of the accuracy of geopotential height measurements.

An experimental study of the errors associated with geopotential height measurements in the atmosphere is complicated by the synoptic variability of the atmosphere itself. Ideally, one would like to estimate the error associated with a measurement technique by taking many measurements of a static system and establishing a bias and a standard deviation from a normal distribution of measurements. The atmosphere, however, does not afford such a simplistic approach. In the case of radio occultation, the best one can do is compare the measurements of geopotential height from GPS/MET data to the output of a global atmospheric model (Lorenc 1981, Shaw et al. 1987). In an arrangement with the European Centre for Medium-range Weather Forecasts (ECMWF), output from their global model is used as the source for comparison in this paper.

The ability of this geopotential height measurement technique to impact climate studies is investigated in the absence of prior knowledge. In this case, it is necessary to implement a scheme to interpolate point measurements at random positions on the globe to create a map. Since the measurement error is unknown, one must have a rigorous way to determine the errors associated with the interpolation and any component of it, such as a global average geopotential height. Bayesian analysis (e.g. Press 1989) is well suited to such a task. In this paper, a Bayesian interpolation technique (MacKay 1992), pioneered in the neural networks community, is used to create such maps. This technique permits one (1) to approximate the error associated with each measurement, (2) to determine the most probable horizontal resolution obtainable with the data, and (3) to perform a rigorous error analysis on the various components of the map it generates. No climatological phenomenon is addressed or analyzed in this paper because of the limitations of the data involved.

The second section of this paper is a brief explanation about GPS radio occultations. Half of the second sections deals with the limitations of this particular data set while the other half lays out how geopotential heights are determined. The third section is a presentation of a comparison of geopotential heights computed from GPS/MET data with those generated by the ECMWF global model. This is similar to the analysis of Kursinski et al. (1996b) but for geopotential heights rather than temperatures. The fourth section is a presentation of maps of geopotential height at constant pressure generated by Bayesian interpolation. In it is discussed how synoptic variability affects global mean quantities. Finally, the fifth section is a summary of results and their implications.

2. Radio occultation with GPS

The technique of radio occultation has been used frequently in the field of planetary science, primarily because it has been the most reliable and accurate method of obtaining temperature profiles in the atmospheres of other planets. Other papers contain more complete descriptions of issues pertinent to using GPS to perform radio occultations, but it is necessary to bring out some of the salient points.

Radio occultation by GPS takes advantage of the refractive properties of the atmosphere by measuring the angle through which the atmosphere bends a radio beam whose source is a GPS satellite. With a GPS receiver aboard GPS/MET, the rate of change of the optical path between the transmitter and receiver is measured. Given accurate knowledge of the positions and velocities of the transmitter and receiver, and assuming spherical symmetry of the atmosphere, one can simultaneously determine the impact parameter a of the radio beam and the angle α through which it was bent on its trajectory from the transmitter to the receiver. This information is directly invertible to a profile of the index of refraction and hence temperature (Fjeldbo et al. 1971).

In the case of GPS/MET, and perhaps most future orbiting GPS receivers intended for radio occultation measurements, the on-board clock is unstable enough to degrade information on both the bending angle and the impact parameter (Hardy et al. 1994). Furthermore, the transmissions of GPS satellites are intentionally dithered (commonly called "selective availability") so that illsl:illtzllt('oils positioning systems (without access to the confidential algorithm for the selective availability) have accuracies worse than 100 meters (Spilker 1980). Hence, a "double-difference" technique has been incorporated to eliminate the effects of the on-board clock noise and the selective availability. This technique requires a GPS receiver with an exceptional clock on the Earth's surface which records the transmissions from *two* GPS satellites during an occultation. One of these satellites is the occulted satellite and the other is a reference satellite.

A consequence of this system is that an occultation is recorded only when a ground GPS receiver is "in view" of an occulted and a reference GPS satellite. During the spring and summer of 1995, only five ground receivers were available: in Pasadena, California; in Kokee Park, Hawaii; in Fairbanks, Alaska; in Tidbinbilla, Australia; and in Potsdam, Germany. It will be clear that the sparse coverage provided by the available ground receivers leaves vast regions of the globe unsampled by occultations from GPS/MET.

A second consequence of this system is that the data provided by GPS/MET is limited in time. In general, the United States Air Force (USAF) imposes a confidential pseudo random code (the "y-code") at a frequency of 10.23 MHz on the GPS satellite transmissions which corrupts an ionospheric correction necessary for eliminating the refractive effects of the ionosphere (Spilker 1980). On occasion, the USAF switches to a known pseudo random code (the "p-code"), which permits an accurate ionospheric correction. Specifically for the GPS/MET project, the USAF switched to p-code three times during 1995, each for a duration of about two weeks. The first period was late April/early May (spring), the second period was late June/early July (summer), and the third period was mid-October (fall). These periods are also known as "anti-spoofing off" (AS-off) periods, and the y-code modulation is known as "anti-spoofing." Only data from the spring and summer AS-off periods are analyzed in this work.

The water vapor/neutral density ambiguity (Kursinski et *al.* 1995) remains unresolved in this work, so any place where the ambiguity becomes substantial is

eliminated from this analysis. The technique of Kursinski et al. (1996a) is adopted, wherein the tropospheric portion of retrievals where the temperature is larger than 250 K is eliminated. It is under this condition that the atmospheric water vapor content generally becomes large enough such that, whenever the flight receiver was even able to track the GPS signal, errors in knowledge of the water vapor content lead to retrieved temperature errors larger than 1 K.

The bending angle as a function of impact parameter, $\alpha(a)$, is inverted via an Abel transform to give the index of refraction as a function of altitude, $n(z)$ (Fjeldbo et al. 1971). All the elements of the occultation inversion are the same as used in Kursinski et al. (1996a), except the determination of geopotential heights. The geopotential heights are determined using the gravity model JGM-3 (Tapley et al. 1996), wherein the altitude z is converted to a potential energy, U. This version of the JGM-3 model is a 64'th degree spherical harmonic expansion which calculates geoids with an accuracy of less than 1 meter. The potential energy includes the effects of the gravitational potential and the centrifugal potential (Gill 1982). The potential energy is then converted to geopotential height by subtracting a constant, which corresponds to the potential energy of "mean sea level," and dividing by a standard gravitational acceleration:

$$h(z) = (U(z) - U_{\mathrm{msl}})/g_0 \tag{1}$$

in which $h(z)$ is the geopotential height, $U_{\mathrm{msl}} = 6.26368525 \times 10^7 \mathrm{m}^2\ \mathrm{s}^{-2}$, and $g_0 = 9.80665\ \mathrm{m\ s}^{-2}$ (John Eyre, private communication). The index of refraction is converted to density ρ by a standard relation (cf. Eq. 1 in Hardy et al. 1994). Pressure as a function of geopotential height is then computed using the hydrostatic equation:

$$p(h) = \int_h^{\infty} \rho(h')\, g(h')\, dh'. \tag{2}$$

The units of geopotential height h are geopotential meters ("gpm") or geopotential kilometers ("gpkm") so that one is reminded that h is not a true length.

3. Comparison of occultations to ECMWF model

The output of the ECMWF global model (cf. Lorenc 1981, Shaw et al. 1987) contains temperatures and humidities at 31 atmospheric levels which span the troposphere and lower stratosphere, the pressure at the interfaces of each layer, and the surface geopotential, all as functions of latitude and longitude. The horizontal resolution is 1 degree by 1 degree over the globe. The layers are counted from the the top downward. The topmost few layers are defined by constant pressure coordinates, and the bottommost few layers are defined by constant sigma, or pressure divided by surface pressure coordinates. The middle layers are mixed pressure-sigma coordinates. The topmost layer spans 0 to 200 millibars and the bottommost layer abuts the surface.

In order to compute the geopotential height profile given the ECMWF output, the hydrostatic equation is integrated. Defining $p_{i-1/2}$ as the pressure at the top of layer i, T_i as the temperature of the layer i, q_i as the water vapor mass fraction of layer i, and $h_{i-1/2}$ as the geopotential height at the top of layer i, then

$$h_{i-1/2} = h_s + \frac{1}{g_0} \sum_{j=i}^{31} RT_j \left[\frac{q_j}{\mu_{\mathrm{water}}} + \frac{1-q_j}{\mu_{\mathrm{dry}}} \right] \log\left(\frac{p_{j+1/2}}{p_{j-1/2}} \right) \tag{3}$$

where the ideal gas constant $R = 8.3143$ J K^{-1} mol^{-1}, the molecular mass of dry air $\mu_{\rm dry} = 28.964$ gm mol^{-1} (Houghton 1986), and the molecular mass of water $\mu_{\rm dry} = 18.0$ gill 11101-^{1}. Implicitly, $p_{j+1/2}$ for $j = 31$ is the sul'face pressure and h_s is the geopotential height of the surface used by ECMWF. Given this profile, geopotential heights as a function of pressure are interpolated linearly in the logarithm of the pressure.

As a first s{(]) in investigating the accuracy of the retrievals of geopotential heights, a statistical analysis of the differences of geopotential heights between the retrievals and the ECMWF output is done. The difference $\delta h(p)$ is defined as the difference between the retrieved geopotent i a] height as a function of pressure, $h_{\rm retrieved}(p)$, and the 11)() (1('1 geopotential height as a function of pressure, $h_{\rm model}(p)$:

$$\delta h(p) = h_{\rm retrieved}(p) - h_{\rm model}(p). \tag{4}$$

This calculation is done for each occultation, retaining a mean difference, $\overline{\delta h}(p)$, and a standard deviation, $\sigma_{\delta h}(p)$.

These statistics have been done for the occultations in 3 days during the spring and 10 days during the summer. Figure 1 shows the number of occultations successfully processed for each day in the spring 1995 and summer 1995 AS-off periods. For four days of the 20 day AS-off period during the spring of 1995, GPS/MET provided good sets of occultations: 24 April, 25 April, 4 May, and 5 May. Several more days during the summer AS-off period provided good sets: 21 June 24 June, 27 June 3 July. Output from the ECMWF global model was only obtained for 25 April, 4 May, 5 May, 21 June 23 June, 27 June 3 July, though. All told, 149 occultations were succesfully obtained and compared to ECMWF during the spring and 579 during the summer.

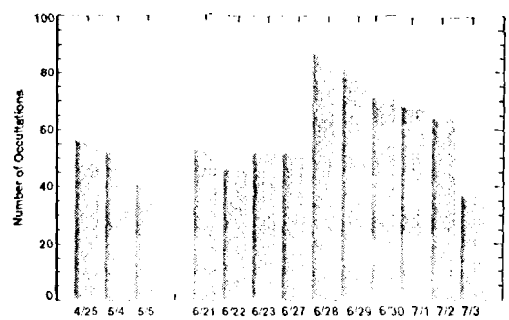

Fig. 1. The number of occultations for each (lay used in comparison with the ECM \\ 'P global model output. The histogram is split between the spring and the summer sets in 1995.

The statistical results are shown in figures 2 and 3. The profiles have been separated according to their latitude before the statistics were calculated. All occultations occuring above 30°N are northern, all occultations occuring between 30°S and 30°N are tropical, and all occultations occuring below 30°S are southern. This was done because the ECMWF model performance is expected to differ according to the region. The central solid curve in each plot is the mean difference $\overline{\delta h}(p)$, and the shaded region is the standard deviation $\sigma_{\delta h}(p)$ about the mean difference. The mean difference is plotted with associated error bars, defined as the standard error. The

standard error is calculated by dividing the standard deviation by the square root of the number of contributing profiles less one. Because of the large number of profiles obtained during the summer, the error bars are hardly visible beneath the bias curve. The Statistics do not extend as deeply into the troposphere in the tropics as in the north or south because of the presence of water vapor.

In a geopotential height statistical comparison, the biases in the temperature are related to slopes in the bias of the geopotential, but it is difficult to relate the standard deviations, or measurement error. If a temperature bias as a function of pressure is written as $\delta T(p)$, then the geopotential bias can be given, assuming hydrostatic balance, as

$$\delta h(p) = \int_{p}^{p_{surface}} \frac{R\,\delta T(p')}{\mu g_0} \frac{dp'}{p'} \tag{5}$$

where R is the ideal gas constant and μ is the mean molecular mass. Thus the biases in the statistical results of Kursinski et al. (1996a) can be easily ranged to the biases in the statistics of the geopotential heights. Relating the standard deviations is more difficult, though, because it is not known to what degree the temperature differences are vertically correlated. If temperature errors are highly vertically correlated, then errors in the geopotential would be more exaggerated. On the other hand, if temperature errors are vertically uncorrelated, then errors in the geopotential would be [illegible] less.

The bias in the northern hemisphere during the spring indicates that measured temperatures were persistently cooler than in the model, whereas no such temperature bias occurs during the summer. In the spring, a bias of about -30 gpm exists at 40 millibars and no bias at 600 millibars with a steady trend in between. This trend results from measured temperatures being 0.4 K cooler than in the model in this layer. No such trend is apparent in the northern hemisphere during the summer, but a constant bias of 15±2 gpm is apparent.

The bias in the tropics during the spring shows the effect of substantial wave activity about the tropopause, whereas the lower biases in the summer indicate less wave activity. Kursinski et al. (1996a) show a dramatic wave structure in the tropics during the spring, which creates the large bias and standard deviation in the geopotential heights around and above the tropopause (at $\sim$ 100 millibars). The bias in the summer data, however, is essentially nonexistent, indicating that any wave structure may not have been as large during the summer as during the spring.

The bias in the southern hemisphere shows that the model has difficulty in retrieving the temperature/pressure structure in the vicinity of the tropopause. For both the spring and the summer, the bias is nearly vertical above and below the tropopause, but it is sloped in the intermediate region. This may result from the model placing the tropopause higher than did the occultation measurements. The reason for this would be that the model has very few radiosonde measurements to assimilate in the southern hemisphere.

The variance in this statistical comparison, $\sigma^2_{\delta h}$, is really the sum of the squares of the analysis error of the model and of the occultation measurement error: $\sigma^2_{\delta h} = \sigma^2_h(\text{model}) + \sigma^2_h(\text{measurement})$. Thus, the statistical comparisons shown here can only give an upper bound on the measurement error. One can show where the model is likely to perform less well, however, since the model error is assumed to be dependent on position while the measurement error is not.

The standard deviations about the bias are minimized in the northern hemisphere and the tropics while the variances are enhanced in the southern hemisphere.

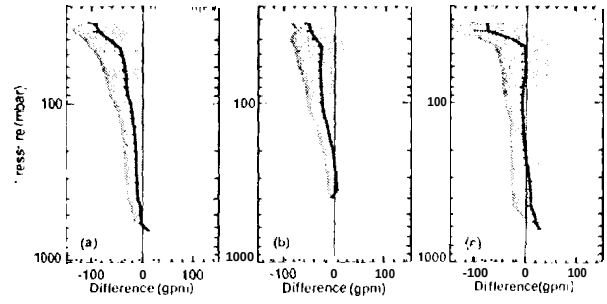

Fig. 2. Comparison of occultation geopotential heights to ECMWF for spring 1995. The mean difference between geopotential heights retrieved from occultations and those in the model output is shown as a function of pressure. The solid central curve shows a mean bias. Positive differences mean that the occultations measured higher heights than did the model. The cross hatches indicate the error in the mean bias. The shaded region indicates the range of differences within one standard deviation of the mean difference. In (a) 52 occultations from latitudes greater than 30°N are compared. In (b) 52 occultations between 30°S and 30°N are compared. In (c) 45 occultations below 30°S are compared.

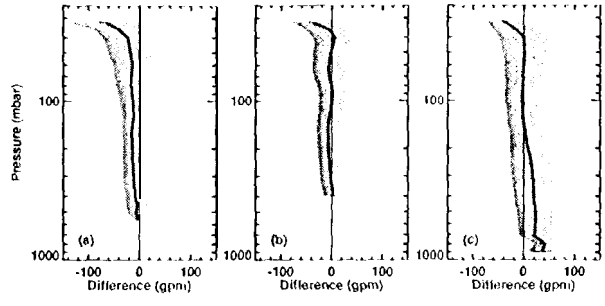

Fig. 3. Comparison of occultation geopotential heights to ECMWF for summer 1995. Same as for figure 2, but for summer 1995. In (a) 222 occultations are used In (b) 193 occultations are used. In (c) 164 occultations are used.

During the spring, the standard deviation in the northern hemisphere and the tropics below 100 millibars is 20 to 30 geopotential meters while in the southern hemisphere it is 30 to 40 geopotential meters. During the summer, the standard deviation in the northern hemisphere and the tropics below 100 millibars is 20 geopotential meters while in the southern hemisphere it is 30 to 40 geopotential meters. This demonstrates that the model error is at most 20 geopotential meters and that the ECMWF model has larger analysis errors in the southern hemisphere than in the tropics or northern hemisphere. This could be a consequence of there being fewer daily balloonsonde soundings in the southern hemisphere than elsewhere.

(a)

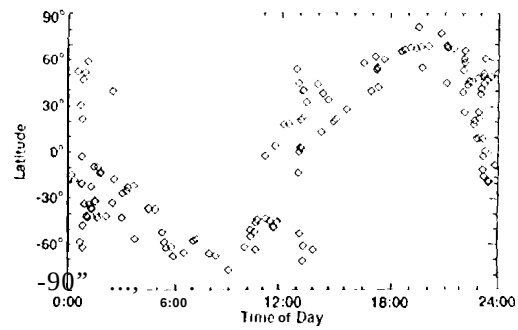

(1))

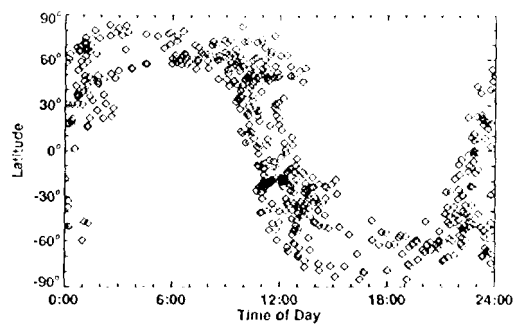

Fig. 4. Spatial-temporal bias of the data. The latitude of the occultation is plotted versus the local time of day for the occultations used in the (a) spring and (b) summer comparisons.

The statistics in figures 2 and 3 may be biased by the temporal and spatial sampling of the occultations. During both the spring and the summer AS-off periods, GPS/MET was in a nearly sun-synchronous orbit with an inclination of $\sim 70°$. As a result, during the spring the northern occultations occured between noon and midnight and the southern occultation occured between midnight and noon (figure 4a). During the summer, the northern occultations occurred between midnight and noon and the southern occultations occurred between noon and midnight (figure 4b). Because the measurements are somewhat cooler than the model output in the north during the spring and in the south during the summer, the model appears to generate tropospheric temperatures which are too warm, by half a degree or less, in the afternoon.

4. Mapping geopotential heights

In this section, a map of the geopotential heights of constant pressure surfaces is constructed in order to qualify how effectively radio occultation measurements can characterize the geopotential height field. Radio occultations are unique in that they sample the atmosphere approximately randomly across the globe (except for the time-of-day effect obvious in figure 4). Thus the data must be interpolated in order to create a map. In addition, the best data acquired contributed only ~ 70 measurements per day; therefore, several days of data must be grouped together to create any Ills]). The atmosphere is variable over such long time periods, which contributes additional noise when creating a map. This additional noise term is known to vary as a function of location on the globe and as a function of height. A Bayesian interpolation method which can determine "most probable" fits is the most appropriate method to handle data with such characteristics (MacKay 1992).

4.1 Bayesian interpolation

This Bayesian interpolation technique can be approached as an advanced least-χ^2 method. For a simple least-χ^2, one assumes a set of basis functions, which are spherical harmonics in this work (Morse and Feshbach 1953, Press et al. 1986), and adjusts their coefficients such that the square of the difference between the fit and the data is minimized. If ϕ_{ij} is the evaluation of the j'th basis function at the location of the i'th data point, then the vector of "most likely" coefficients $\mathbf{w}_{ml}$ which minimizes χ^2 is simply

$$\mathbf{w}_{ml} = \mathbf{B}^{-1}\phi^T\mathbf{t} \tag{6a}$$

where

$$\mathbf{B} = \phi^T\phi \tag{6b}$$

and $\mathbf{t}$, is the data vector. One generally implements constraints on the fit by introducing a penalty function (Daley 1991) in the form of a diagonal matrix $\mathbf{C}$. Usually, this penalty function favors smooth fits by placing increasing elements on the diagonal of $\mathbf{C}$. It is necessary then to weight the penalty function, and this is done by

$$\mathbf{A} = \beta\mathbf{B} + \alpha\mathbf{C} \tag{7}$$

where α and β are the weights. With this constraint, the set of "most probable" coefficients $\mathbf{w}_{mp}$ becomes

$$\mathbf{w}_{mp} = \mathbf{A}^{-1}\beta\phi^T\mathbf{t}. \tag{8}$$

Notice that $\mathbf{A}\mathbf{w}_{mp} = \beta\mathbf{B}\mathbf{w}_{ml}$, and thus the effect of constraining the fit is to reduce the higher order coefficients. The determination of the most probable coefficients is called the first inference in Bayesian interpolation.

The second inference in Bayesian interpolation involves selecting the most probable values for α and β. This selection cannot be done with orthodox statistics. The most probable values for α and β satisfy the criteria

$$\alpha = \gamma\left(\mathbf{w}_{mp}^T\mathbf{C}\mathbf{w}_{mp}\right)^{-1} \tag{9a}$$

$$\beta = (N-\gamma)\left(|\mathbf{t} - \phi\mathbf{w}_{mp}|^2\right)^{-1} \tag{9b}$$

in which N is the number of data points and γ is the number of "effective" free parameters of the fitted model. The term $\mathbf{w}_{\rm mp}^{\rm T}\mathbf{C}\mathbf{w}_{\rm mp}$ in equation (9a) should be recognized as the size of the penalty, and the term $|\mathbf{t} - \phi\mathbf{w}_{\rm mp}|^2$ in equation (9b) should be recognized as the misfit of the data. The number of effective free parameters, γ, is slightly less than the number of basis functions, k, used in the fit. γ is determined by

$$\gamma = k - \alpha\,{\rm Tr}(\mathbf{A}^{-1}\mathbf{C}) \tag{10}$$

in which Tr(...) takes the trace of a matrix. The rightmost term in the above equation is understood as counting the number of parameters discarded by the penalty function. Equations (7), (8), (9), and (10) are iterated in α and β until all are satisfied.

The determination of the data weight β can be understood given a simple example. Assume that one is to measure a single fixed scalar quantity N times. No smoothness condition is necessary, so no penalty function such as one described above is implemented. The obvious best fit to the data would be the average of the data. Because there is one free parameter ($\gamma = 1$), the value for β given by equation (9b) is

$$\beta = 1/\sigma^2 \tag{11a}$$

where

$$\sigma^2 = (N - 1)^{-1}\sum_{i=1}^{N}(t_i - \bar{t})^2 \tag{11b}$$

in which t_i are the measurements and $\bar{t}$ is their average

An interesting property of this interpolation technique is that the error covariance matrix for the fitted coefficients is simply $\mathbf{A}^{-1}$. Thus, in order to calculate the error at a location $\mathbf{y}$, one only needs to calculate

$$\text{error}(\mathbf{y}) = \left[\phi(\mathbf{y})^{\rm T}\,\mathbf{A}^{-1}\,\phi(\mathbf{y})\right]^{1/2} \tag{12}$$

in which the i'th element of the vector $\phi(\mathbf{y})$ is the evaluation of the i'th basis function at the position $\mathbf{y}$ of the interpolated point. This error estimate is assuredly real valued because both $\mathbf{A}$ and its inverse are positive definite.

The technique of MacKay (1992) also permits for the determination of the most probable model. In this paper, the different models are created by adding higher degree spherical harmonics to the basis set. Model number n uses n degrees of spherical harmonics as basis functions. For n degrees, $k = (n+1)^2$ basis functions are used. In evaluating the probability of each model, each is rewarded according to its ability to fit the data and is penalized according to the number of effective free parameters it uses. Since prior knowledge of the atmosphere dictates that it has significant structure at very small scales, the most appropriate penalty function must not penalize models that allow for very fine horizontal resolution. This step in Bayesian interpolation is called the third inference. For a detailed explanation of this procedure, see MacKay (1992).

In this analysis, the data $\mathbf{t}$ are the geopotential heights at a given pressure, the positions $\mathbf{x}_i$ are the latitude and longitude of each occultation, and each element of the projection matrix ϕ is defined by

$$\phi_{ij} = Y_m^l(\mathbf{x}_i) \tag{13}$$

model degree	α	β	log(model probability)
1	1.129	7.359	306.449
2	0.8789	41.87	851.957
3	0.3995	102.4	1122.45
4	0.2817	138.6	1206.71
5	0.08948	159.9	1228.65
6	0.07579	174.6	1246.41
7	0.07628	179.3	1248.95
8	0.07458	187.9	1258.78
9	0.07156	94.1	1264.68
10	0.07202	95.6	1265.08
11	0.07239	96.2	1264.55
12	0.07387	96.7	1264.94
13	0.07607	96.3	1264.36
14	0.0777s	96.0	1263.89

Table 1. Model probabilities and statistics from Bayesian interpolation of the 100-mbar surface, summer 1995.

in which j uniquely identifies each l, m pair. The function Y_m^l is the spherical harmonic of degree l and order m. The penalty function is chosen such that the high degree fits are all equally probable. With a trial formulation for the penalty matrix $\mathbf{C}$, the probability, the weights α, β, and the fitted coefficients w_{mp} are solved for using equations (8), (9), and (10). If all the high degree models are not equally probable, then another formulation for the penalty matrix is assumed and the testing process is repeated. When a suitable penalty function is found, then maps of the data are created using the most probable coefficients for a high degree fit.

An appropriate penalty function must take two pieces of prior knowledge into account. First, the term in the series which corresponds to the global mean ($l = 0$, which implies $m = 0$) must be weighted much less than the others because it is expected to be much larger than any other term in the series. Secondly, the terms which represent purely meridional structure ($l \neq 0, m = 0$) must be weighted less than those with zonal structure ($l \neq 0, m \neq 0$) because meridional gradients in the Earth's atmosphere are expected to be much stronger than zonal gradients. With these considerations, an appropriate form of the penalty matrix turns out to be

$$C_{jj} = \begin{cases} 1/1000, & \text{for } l = 0 \\ l^3(l+1)^3/100, & \text{for } l \neq 0, m = 0 \\ l^3(l+1)^3, & \text{for } l \neq 0, m \neq 0. \end{cases} \tag{14}$$

To show that higher order models are all equally probable with this formulation for the penalty function, the probabilities along with several other fitted quantities are listed in table 1. In generating this table, the geopotential height for the 100-mbar pressure surface was interpolated given the occultation data set obtained during the summer.

4.2 Geopotential maps

Figures 5a-d show maps of the geopotential heights of the 100-, 200-, 300-, and 400-mbar surfaces during the summer. The location and height of each occultation

is given by a color-coded point on each map. In each case, the fit is done with a degree 12 spherical harmonic, which requires 169 coefficients. This fit is equivalent to grouping the data into 30° bins and averaging. This resolution is chosen so that the fit oversamples regions where there is little data. With this particular interpolation technique, oversampling will appropriately show little structure where there is sparse data and correspondingly increase predicted error in these regions. At 100 millibars, 641 measurements were interpolated; at 200 millibars 637 measurement were interpolated; at 300 millibars 635 measurements were interpolated; and at 400 millibars 411 measurements were interpolated. At 400 millibars, most of the tropical occultations are not included because of the presence of water vapor.

4.2.1 Measurement accuracy

Table 2 contains a list of the measurement uncertainties $\beta^{-1/2}$, the global average geopotential height $w_{\mathrm{mp},0}$, and its associated error. Because approximately two weeks of data are collapsed onto one map, the synoptic variability contributes to the predicted error. Since the occultation measurements agree to within 30 gpm with the ECMWF global model, any predicted interpolation error greater than 30 gpm is caused by temporal variability of the atmosphere. The single measurement error as determined by the interpolation, σ_{interp}, which is given by $\beta^{-1/2}$, is well in excess of 30 gpm because of the temporal variability. In fact, the quantities given in table 2 represent a global average synoptic variability.

The synoptic variability is globally nonhomogeneous, however. The zonal average component of the fit at 300 millibars is shown in figure 6. It is apparent in this plot that the tropical latitudes are much less variable than are the higher latitudes. The variability is approximately 200 gpm around 60°S and is approximately 30 gpm between 20°S and 20°N. Some of this variability arises from features which were stationary over two weeks, but most of it arises from horizontally propagating features. It is known that synoptic variability is depressed in the tropics (Peixoto and Oort 1992).

It is also evident that the best interpolation technique should require a measurement error which is position dependent. In this analysis, it is assumed that the interpolation measurement error is independent of technique and can be completely described by the scalar weight β. Since in fact much of the interpolation measurement error σ_{interp} is composed of atmospheric variability, which is itself intensely position dependent, it would be most appropriate to construct an interpolation measurement error, and hence β, which is dependent on position.

One consequence of the single-valid interpolation measurement error is that the error bars in figure 6 are larger in the tropics than in the midlatitudes. The sizes of the error bars are roughly the interpolation error σ_{interp} divided by the square root of the number of points in a 30° latitude bin. The errors bars are larger in the tropics than at midlatitudes because there are fewer measurements in the tropics than at midlatitudes. In truth, though, the decreased variability in the tropics should make the error bars in the tropics smaller than at midlatitudes.

4.2.2 Atmospheric features

The dominant structures in each of these maps is the inter-hemispherical asymmetry and the equator-to-pole gradients. In each of the maps, there is a strong geopotential equator-to-pole gradient in the southern hemisphere with while the gradient is

(a)

Height of 10Omb Surface, Summer AS-off Period

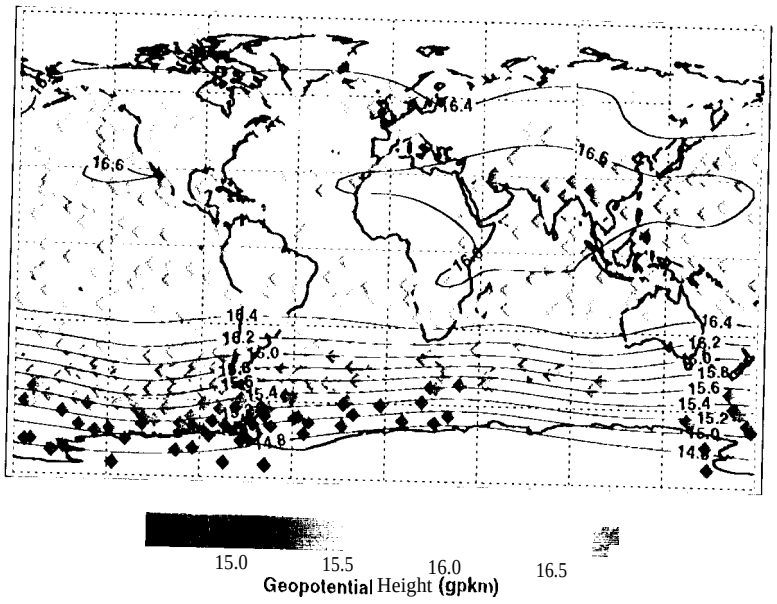

(1))

Height of 200mb Surface, Summer AS-off Period

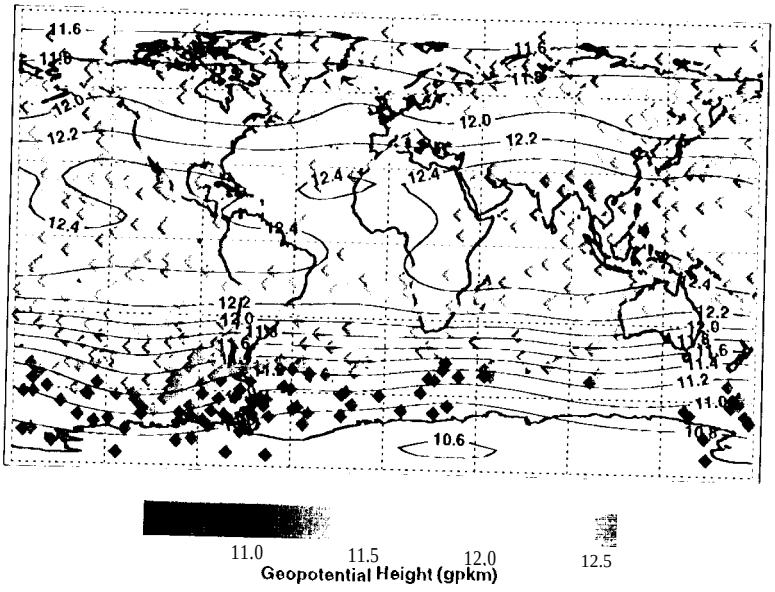

Fig. 5. Geopotential height maps of constant pressure surfaces, summer 1995. Contour maps of the geopotential heights are overlaid upon the data available. The data is located and color-coded according to the occultation locations and the retrieved geopotential height. Each map is a twelfth-degree spherical harmonic Bayesian interpolation of the data available. Contours are separated by 0.2 gpkm. (a) 100-mbar surface, (II) 200-mbar surface, (c) 300-mbar surface, (d) 400-mbar surface.

(c)

Height of 300mb Surface, Summer AS-off Period

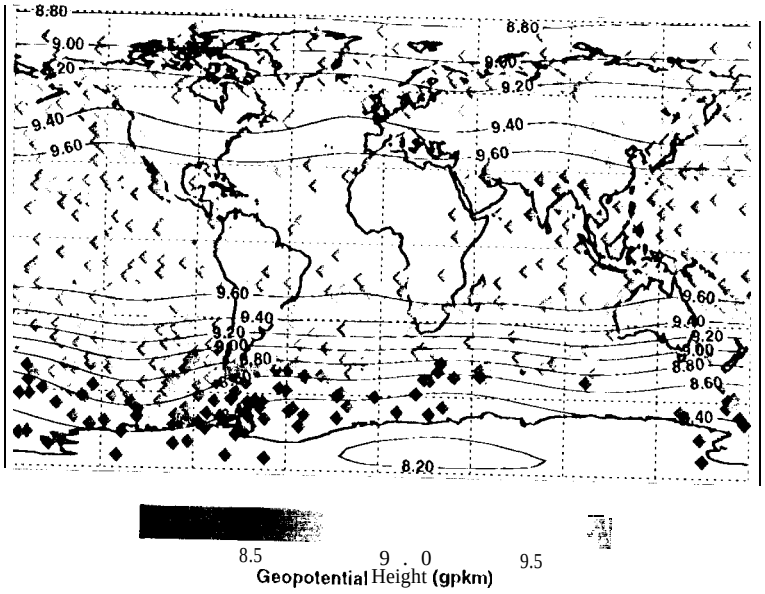

(d)

Helght of 400mb Surface, Summer AS-off Period

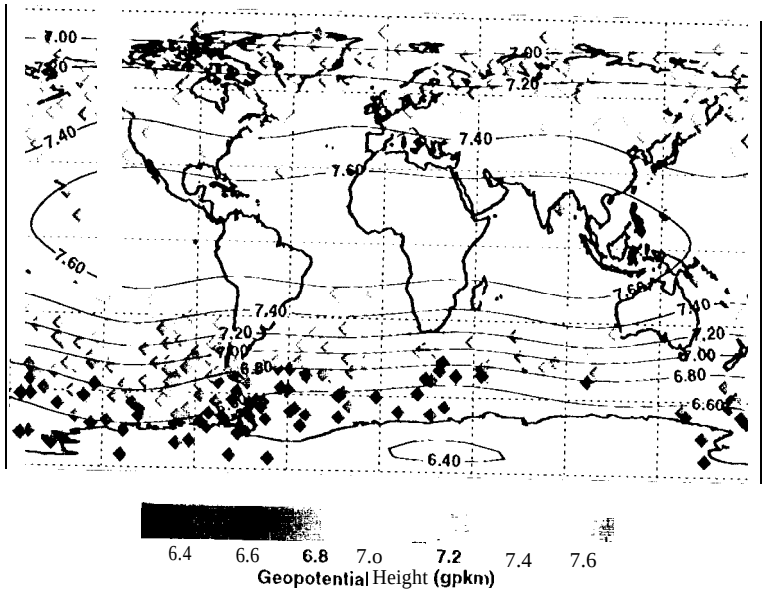

Fig. 5. continued.

pressure (millibars)	measurement error (gpm)	global average height (gpkm)
100	71.3	16.3153 ± 0.0041
200	101.8	12.04383 0.00,58
300	117.8	9.37134 **0.006,5**
400	125.6	7.3595 ± 0.0226

Table 2. Interpolation measurement error and the global average height of constant pressure surfaces, summer 1995. The interpolation measurement error, which is composed of single measurement error and atmospheric variability, is given as a function of pressure. In addition, the global average geopotential height with an associated uncertainty is also given. These quantities are extracted from a Bayesian interpolation using a twelfth degree spherical harmonic as the basis.

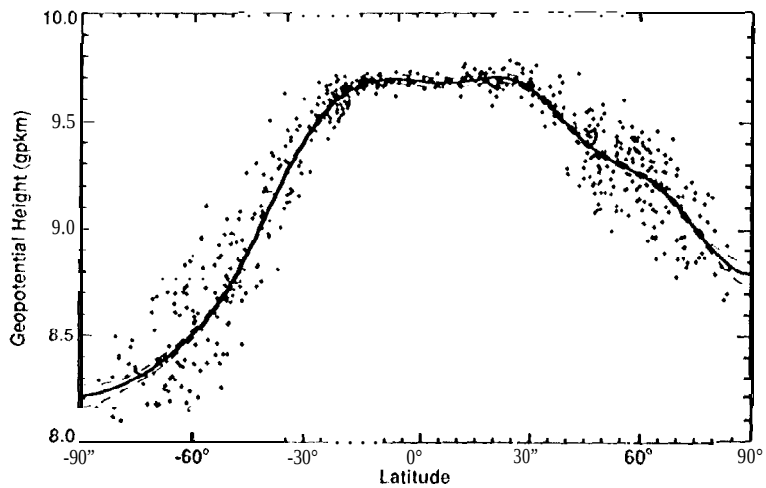

Fig. G. Zonal average geopotential height of the 300-mbar surface, summer 19!35. The zonal average component of the map shown in figure 5c is plotted as a function of latitude. The region within error of the average falls within the dashed lines. The data are plotted as individual points.

much weaker in the northern hemisphere. This is expected since the southern hemisphere is the winter hemisphere. The southern gradient grows stronger with increasing altitude, a consequence of higher latitudes being colder than lower latitudes.

At 100 millibars, though, the equator-to-pole geopotential gradient is much smaller than at lower altitudes. The difference in geopotential height between the north pole and the tropics is approximately 800 900 gpm at 2?00 **400** millibars whereas it is approximately 300 gpm at 100" millibars. Since the geostrophic zonal wind u_g is related to the meri dional geopotential height gradient by

$$u_g = -\frac{g_0}{2\Omega R_e \sin\theta}\frac{\partial h}{\partial \theta} \tag{15}$$

in which $\Omega = 2\pi/(24\text{hrs})$, θ is latitude, and R_e is the radius of the Earth, the northern midla titude jet is smaller at 100 millibars than at 200" to **400** millibars by 60%. The

mechanism for the decay of winds is most likely the radiative heating of the lower atmosphere in the Northern Hemisphere.

The most prominent zonally asymmetric feature is a local high over the southeastern Pacific, which is most likely the quasi-stationary wave known to persist throughout the annual cycle (Will Loon and Jenne 1972, Quintanar and Mechoso 1995). A cross-section of the 300-mbar geopotential height map at 60°S latitude is shown in figure 7. The average of the ECMWF model output over the same time period is also shown. The geopotential height at 120°W is elevated by approximately 250 gpm in comparison with the zonal average. At the same location the error estimate is 25 gpm. The high at 120°W is the same in the ECMWF model output. There is a weaker high and a low at 112°1", and 45°E, respectively. The model average shows a high and a low in the same locations, except 11101'(" pronouncedly. That the interpolation does not accurately account for the heighth and depth of these two features is reflected in the size of the error bars: the increase in error is a consequence of a local paucity of data.

Some less prominent features of zonal asymmetry appear in the northern hemisphere, but they are not positive detections of a real stationary feature. Figure 8 shows a similar cross-section but at 40°N latitude. The wavenumber 3 component of this cross-section has an amplitude of 46 ±20 gpm; but because the local variability is significantly underestimated at all midlatitudes, this is probably only slightly greater than a one sigma detection. Indeed, the ECMWF model average shows no definite wavenumber 3 structure at this latitude.

4.3 Position dependent bias

In all of the previous interpolations, only the occultation data was considered. The interpolation technique determined an interpolation measurement error σ_{interp} which reflected a global average measurement error. This does not accurately reflect the nature of the data because the atmospheric variability effectively makes σ_{interp} position-dependent.

This version of Bayesian interpolation is better suited to mapping the occultation observations with the variability removed. If one assumes that the ECMWF global model accurately reproduces the model variability, then the variability can be removed from the observations by subtracting the relevant quantity from the ECMWF model output from the occultation observation. The profile taken from the model output coincides with the occultation to within three hours and is bilinearly interpolated in position. By interpolating the residual, a map of the bias between the ECMWF global model and the radio occultations is produced.

The interpolation measurement error in this case is slightly position dependent, but not as much as in the previous interpolations. The global model is known to be less accurate in some regions than others as a consequence of data availability. This would make σ_{interp} position dependent, but by removing the atmospheric variability, the largest source of position dependence is eliminated.

The penalty function then becomes less complicated than the previous. Because the difference between the observations and the model output is not expected to have any position dependent structure, no specialized weighting in the penalty function is necessary. In fact, a penalty function which minimizes curvature is all that is necessary:

$$C_{jj} = \begin{cases} 1 & \text{for } l = 7/l = 0, \\ l^2(l+1)^2 & \text{otherwise.} \end{cases} \tag{1(i)}$$

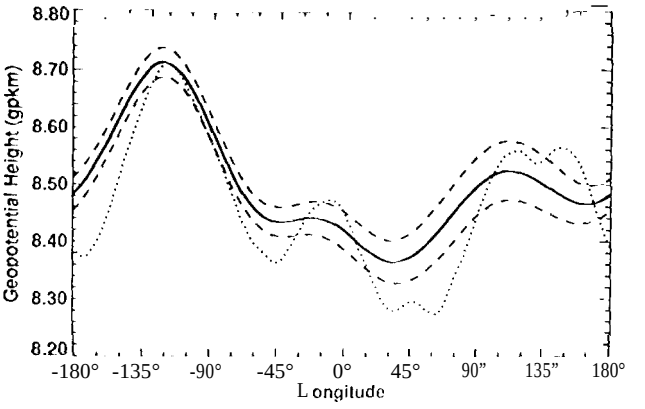

Fig. 7. Geopotential height of the 300-mbar surface at 60°S, summer 1995. A cross-section of the map contoured in figure 5c with error bars given by the dashed lines. The dotted line shows the average geopotential height for the same period and location computed from the output of the ECMWF global model.

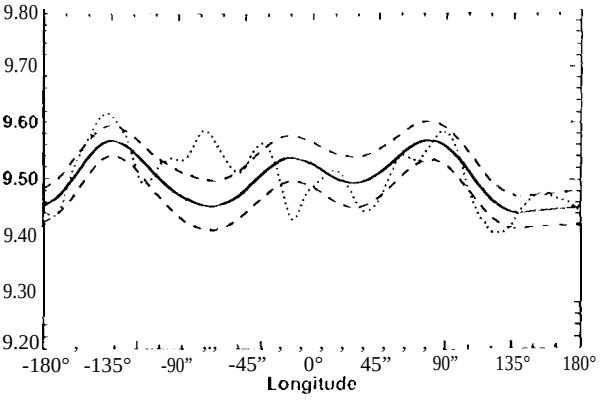

Fig. 8. Geopotential height of the 300-mbar surface at 40°N, summer 1995. Same as figure 1 but at 40°N latitude.

With this penalty matrix, all high order fits are equally probable.

In figure 9, a degree 12 fit to the difference in geopotential height of the 300-mbar surface between the occultation observations and the model output is contoured. Again, this is equivalent to 30° horizontal averaging. The interpolation measurement error is 27.4 gpm, similar to the halfwidth at 300 mb given in figures 2 and 3.

By far the most prominent feature is a bias in the south Pacific centered at 135°W, 60°S. The geopotential height at 300 millibars as determined by the occultations is approximately 50 gpm higher than given by the ECMWF global model at this location. This implies that the occultations measured a warmer atmosphere below 300 millibars, consistent with the model placing the tropopause too low in this region

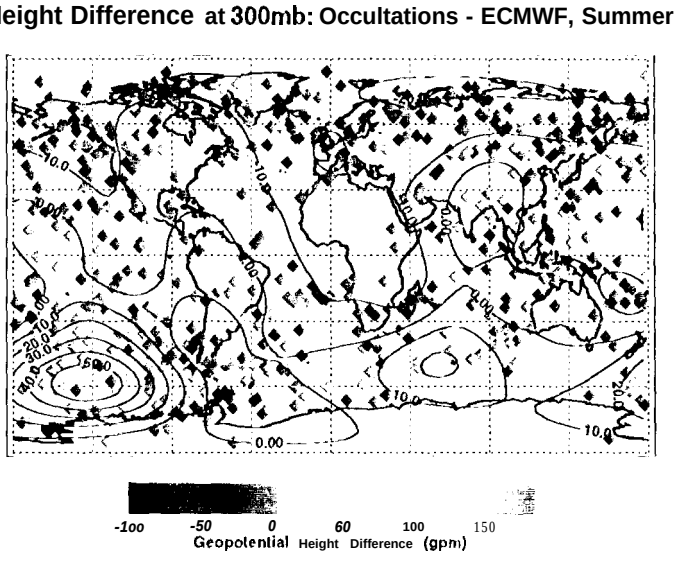

Fig. 9. Map of the geopotential height difference of the 300-mbar surface between that obtained from the occultations and that obtained from the ECMWF global model. A contour map of the difference between 300-mbar geopotential heights obtained from the occultation data and the same given by the ECMWF global model is superimposed upon the difference data. The points are located and color-coded according to the position of the occultation and the geopotential height difference between it and the colocated model quantity. The map is generated by a twelfth degree Bayesian interpolation. Contours are separated by 10 gpm.

as pointed out by Kursinski et al. (1996a).

The occultations show that the 300-mbar surface is higher than in the model output in the southern hemisphere, but lower than in the model output in the northern hemisphere. This is consistent with the statistics in figure 3. Even though the bias is the southern hemisphere is largely caused by the anomaly in the south Pacific, nevertheless there is substantial bias elsewhere in the southern hemisphere. For example, there is a large region of positive bias between 0° and 135°E which peaks at +20 gpm near 60°E in the south. The only slightly negatively biased region in the south lies south of South America where the bias never falls below -10 gpm.

5. Discussion

Previous work with radio occultation of the Earth's atmosphere using GPS has focused on the retrieval of temperature versus pressure. This work utilizes the ability of GPS to do precise positioning to measure the absolute height of constant pressure surfaces. Kursinski et al. (1996b) have theoretically calculated that the geopotential height error is about 7 gpm at 300" millibars. Here an error estimate is made by comparing occultation observations from GPS/MET with output from the ECMWF global model. Also, an attempt is made to determine global average geopotential height during a two week period in the summer of 1995 without the benefit of outside information. Finally, the bias between the occultation measurements and the ECMWF model is determined as a function of position in order to demonstrate that ECMWF model performance is a function of position on the globe.

Only an upper bound can be placed on the error associated with a single measurement of the geopotential height of a constant pressure surface. In this paper, that estimate was performed by comparing occultation measurements to the output of the ECMWF global model, which itself has associated errors. Since the true measurement error must be independent of position, the upper bound on the measurement error is the lowest determine error in the best modeled region of the globe. That region is above 30° N latitude in this work, where the error was found to be approximately 20 gpm throughout the troposphere.

Any attempt to measure geopotential heights regionally or globally without outside knowledge is dependent on synoptic variability. With data from just one orbiting receiver, one can construct an adequate map only if data spanning several days are used as a single set. In this case, because the atmosphere varies dramatically over time, especially outside the tropics, any determination of error per measurement consists largely of the unresolved temporal variability. Nevertheless, during the summer, with over 600 occultations, the global average geopotential height of the atmosphere at 300" millibars is found to be 9,371±17 gpm. The uncertainty takes into consideration the atmospheric variability over two weeks and the spatial nonhomogeneity of the data, but not the spatial-temporal bias. The error decreases with height because more data is available and because variability is less higher in the atmosphere.

GPS/MET by itself cannot be used for regional climate studies. The data from GPS/MET yielded just over 600 observations during a two week period during the summer. Those data are spatially-temporally biased by the fact that only one receiver was used to collect it. Far fewer observations were obtained during the spring. During the fall, however, probably more than 600" observations were obtained, but they remain unaddressed in this work.

A future constellation of orbiting receivers would easily allow for regional and global climate studies. By using many receivers, the spatial-temporal bias would be removed. Furthermore, the increased quantity of data would allow for finer temporal resolution, thus decreasing the synoptic variability which degraded the mapping in this paper. If one assumes that a future orbiting receiver obtains 500 occultations per day, a future constellation of 16 orbiting receivers should be able to measure global average geopotential heights in the troposphere with an accuracy of 1 gpm each day. If one assumes a nearly dry adiabatic lower atmosphere with unchanging mass, the height of the 300-mbar surface expands 30 gpm for every degree of warming. At lower pressures within the troposphere, constant pressure surfaces rise even more. The stratosphere, however, is expected to cool by .11° C because of radiative cooling by carbon dioxide (Fels et al. 1980), and thus its thickness should decrease.

The accuracy of a regional measurement of geopotential heights is dependent on the size of the region and its nature. Naturally, the larger the region, the more observations which can be used in an estimation, and hence the greater accuracy with which geopotential heights can be measured. Secondly, regions with less synoptic variability will yield more accurate geopotential height estimates. For instance, it is evident in figure 6 that the tropics are far less variable than elsewhere, an atmospheric phenomenon which is a consequence of the near absence of planetary vorticity. Since mid-tropospheric temperature increases should be most easily detected in the tropics because of the depressed variability (Hansen et al. 19$ S), one can anticipate that geopotential height increases should also be more easily detected in the tropics.

References

Barnett, 'J'.]'., and M.E. Schlesinger, Detecting changes in global climate induced by greenhouse gases, *J. Geophys. Res.*, *92*, 14,772-14,780, 1987.

Chahine, M.T., N.L. Evans, V. Gilbert, and R.D. Haskins, Requirements for a passive IR advanced moisture and temperature sounder, *Appl. Opt.*, *23*, 979-989, 1984.

Christy, J.R., and R.W. Spencer, Assessment of precision in temperatures from the Microwave Sounding Units, *Climatic Change*, *30*, 97-102, 1995.

Daley, R., *Atmospheric data analysis*, 457 pp., Academic Press, San Diego, 1991

Fels, S.B., J.]). Mahlman, MI), Schwarzkopf, and R. W. Sinclair, Stratospheric sensitivity to perturbations in ozone and carbon dioxide: radiative and dynamical resp011s(', *J. Atmos. Sci.*, *37*, 2266-2297, 1980.

Fjeldbo, G., A.J. Kliore, and V.R. Eshleman, The atmosphere of Venus as studied with the Mariner V radio occultation experiments, *Astron. J.*, *76*, 123-140, 1971.

Gaffen, 1). J.> Temporal inhomogeneities in radiosonde temperature records, *J. Geophys. Res.*, *99*, **3667-3676,** 1994.

Hajj, G., E.R. Kursinski, W. Bertiger, S. Leroy, L. Romans, and J.T. Schofield, Sensing the atmosphere from a low-Earth orbiter tracking GPS: early results and lessons from the GPS/MET experiment, /it in Proceedings of the eighth international technical meeting of the satellite division of the Institute of Navigation, pp. 1167-1174, Palm Springs, California, 1995.

Hansen, J., H. Wilson, M. Sato, R. Ruedy, K. Shah, and E. Hansen, Satellite and surface temperature data at odds?, *Climatic Change*, *30*, 103-117, 1995.

Hansen, J., I. Fung, A. Lacis, D. Rind, S. Lebedeff, R. Ruedy, and G. Russell, Global climate changes as forecast by Goddard Institute for Space Studies three-dimensional model, *J. Geophys. Res.*, *93*, 9341-9364, 1988.

Kursinski, E.R., G.A. Hajj, W.I. Bertiger, S.S. Leroy, 'T'. K. Meehan, L.J. Romans, J.T. Schofield, D.J. McCleese, W.G. Melbourne, C.L. Thornton, 'T'.]). Yunck, J.R. Eyre, and R. N. Nagatani, Initial results of radio occultation) observations of Earth's atmosphere using the global positioning system (GPS), *Science*, *271*, 110'/- 110{1. 1996.

Kursinski, E.R., G.A. Hajj, K.R. Hardy, .1.'1'. Schofield, S.S. Leroy, R. Linfield, 1). J. McCleese, 1).0. Muhleman, L.J. Romans, and R. Zurek, Observing Earth's atmosphere with radio occultaiton measurements using GPS, *in preparation*, 1996.

Kursinski, E.R., G.A. Hajj, K.R. Hardy, and .].'J'. Schofield, Observing tropospheric water-vapor by radio occultation using the global positioning system, *Geophys. Res. Lett.*, *22*, X65-23(X, 1995.

Lambert, S.J., Discontinuities in the long-term Northern Hemisphere 500-mb dataset, *J. Climate*, *3*, 147{)- 1484, 1990.

Lindal, G.F., The atmosphere of Neptune: an analysis of radio occultation data acquired with Voyager 2, *Astron. J.*, *103*, 967-982, 1992.

Lindal, G.F., J.R. Lyons, D. N. Sweetnam, V.R.Eshleman, D.P.Hin sol)> and G.L. Tyler, The atmosphere of Uranus: results of' radio occultation]] measurements with Voyager 2, *J. Geophys. Res.*, *92*, 14987- 15001, 1987.

Lindal, G.F., G.E. Wood, G.S. Levy, J.]). Anderson, D. N. Sweetnam, H.B. Hotz, B.J. Buckles, D.P. Holmes, and P.E. 1)[)11)s, The atmosphere of Jupiter: an analysis of the Voyager radio occultation measurements, *J. Geophys.* lies., *86*, 8721-872,7, 1981.

Lorenc, A.C., A global three-dimensional multivariate statistical interpolation scheme, *Mon. Wea. Rev.*, *109*, 701-721, 1981.

MacKay, D.J.C., Bayesian interpolation, *Neur. Comp.*, *4*, 415-447, 1992.

Morse, P.M., and H. Feshbach, *Methods of Theoretical Physics,* 2 vols., 1,978 pp., McGraw-Hill, 1953.

Press, S.J., *Bayesian statistics: principles, models, and applications,* 237 pp., John Wiley and Sons, New York, 1989.

Press, W.H., B.P. Flannery, S.A. Teukolsky, and W.T. Vetterling, *Numerical recipes: the art of scientific computing,* 818 pp., Cambridge University Press, 1986.

Quintanar, A.I., and C.R. Mechoso, Quasi-stationary waves in the Southern Hemisphere. Part I: observational data, *J. Climate*, *8*, 2659-2672, 1995.

Shaw, D. B., P. Lonnberg, A. Hollingsworth, and P. Unden, Data Assimilation the 1984/85 revisions of the ECMWF mass. and wind analysis. *Quart. J. Roy. Meteorol.* .so(".*,* *113*, 533-566. 1987.

S])('l)('d', I{. \\-.. and J.R.Christy, Precision and radiosonde validation of satellite gridpoint temperature anomalies. Part I: MSU channel 2, *J. Climate*, *5*, 847-857, 1992a.

Spencer, R. W., and J.R. Christy, Precision and radiosonde validation of satellite gridpoint temperature anomalies. Part II: a tropospheric retrieval and trends during 1979 90, *J. Climate*, *5*, 858-866, 1992b.

Spencer, R.W., and J.R. Christy, Precise monitoring of global temperature trends from satellites, *Science*, *247*, 1558-1562, 1990.

Spilker, Jr., J.J., GPS signal structure and performance characteristics, in *Global Positioning System, papers published in navigation, vol.1,* edited by P.M. Janiczek, pp. 29-51. The Institute of Navigation, Washington, D.C., 1980.

Tapley, 1).1)., M.M. Watkins, J.C. Ries, G. W. Davis, W.J. Eanes, S.R. Poole, 11. J. Rim, B.E. Schutz, and C. K. Shum, The JGM-3 gravity model, Submitted to *J. Geophys. Res.*, 1996.

Tyler, G.L., V.R. Eshleman, J.D. Anderson, G.S. Levy, G.F. Lindal, G.E. Wood, and T. A. Croft, Radio science with Voyager 2 at Saturn: atmosphere and ionosphere and the masses of Mimas, Tethys, and Iapetus, *Science*, *215*, 553- 558, 1982.

van Loon, H., and 1/ .L. Jenne, The zonal harmonic standing waves in the Southern Hemisphere, *J. Geophys. Res.*, *77*, 992-1003," 1972.

Wallace, J. M., Y. Zhang, and K.-1]. Lau, Structure and seasonality of interannual and interdecadal variability of the geopotential height and temperature fields in the Northern Hemisphere troposphere, *J. Climate*, *6*, 2063 -20S2, 1993.

Ware, R., M. Exner, 1). Feng, M. Gorbunov, K. Hardy, B. Herman, Y. 1<11[), '1'. Meehan, W. Melbourne, C. Rocken, W. Schreiner, S. Sokolovskiy, F. Solheim, .X. Zou, R. Anthes, S. Businger, and K. Trenberth, GPS sounding of the atmosphere from low Earth orbit: preliminary results, *Bull. A m. Meteor. SW.* > *77*, *1940*> 1996.

Wells, D., *Guide to GPS positioning*, Canadian GPS Associates, Fredericton, New Brunswick, 1987.